Whitmarsh, R.B., Sawyer, D.S., Klaus, A., and Masson, D.G. (Eds.), 1996
Proceedings of the Ocean Drilling Program, Scientific Results, Vol. 149

17. MAGNETIC FABRIC ANALYSIS OF FINE-GRAINED SEDIMENTS, IBERIA ABYSSAL PLAIN[1]

Toshiya Kanamatsu[2]

ABSTRACT

The fabric of fine-grained sediments, cored during Ocean Drilling Program Leg 149 to the Iberia Abyssal Plain, was analyzed using the method of anisotropy of magnetic susceptibility. The purposes of this study were to investigate downcore changes in magnetic fabric, and to determine paleocurrent direction. The general magnetic fabric analysis reveals an oblate shape, with K_{min} axes perpendicular to the bedding plane, which is a typical sedimentary fabric. The magnetic lineation ($L = K_{max}/K_{int}$) remains fairly constant throughout the section. However, the magnetic foliation structure ($F = K_{int}/K_{min}$) shows distinctive variation. Several cases show sharp changes at lithostratigraphic boundaries. Poorly foliated intervals at Sites 897 and 898, where inclination of K_{min} is not parallel to the bedding plane, probably resulted from postdepositional disturbance. For selected data from lithostratigraphic Unit I at Sites 897, 898, and 900, the magnetic lineation represented by the K_{max} axes shows clustering indicative of paleocurrent direction. These data suggest that turbidity currents originated from the eastern continental margin of Iberia during the middle Miocene to late Pleistocene.

INTRODUCTION

Measurements of anisotropy of magnetic susceptibility (AMS) provide information about petrofabric: the orientation of principal axes and the shape represented by parameters calculated by normed principal susceptibilities. In this study, the AMS method was applied to investigate downhole petrofabric changes and paleocurrent directions. AMS in sediments may be developed in two stages, during deposition and after deposition. The first stage occurs during settling of grains on the bottom. During deposition, each grain's minimum length axis falls perpendicular to the bedding plane. As a result, the fabric (well-developed foliation) forms an oblate shape. In cases where water currents are present, the alignment of grains is affected by hydraulic forces. The AMS method has been applied to identify current-induced fabric (e.g., Shor et al., 1984). Lithostratigraphic Unit I at Leg 149 sites consists of terrigenous turbidites, and lithostratigraphic Unit II consists of calcareous turbidites and contourites (Sawyer, Whitmarsh, Klaus, et al., 1994). The inference of current direction can provide information useful for determining the history of sedimentation.

After deposition, the fabric may be affected by compaction, tectonic deformation, bioturbation, and/or migration of fluid and gas. Thus, studies of the fabric can also provide information about postdepositional processes.

METHODS

Samples of muddy and silty sediments were selected from Units I and II of each Leg 149 hole to compare the fabric within a consistent lithology. Samples were limited to fine-grained sediments, first, because fine sediments are appropriate for obtaining a stable paleomagnetic direction, and second, because the rolling of particles on the surface causes the fabric in coarser parts of a turbidite unit to be perpendicular to the flow direction (Tarling and Hrouda, 1993). We expect that magnetic lineations of fine grains will be parallel to the paleocurrent direction. Samples were collected at Sites 897, 898, 899, and 900. The samples were taken using 12-cm^3 plastic cubes. Remanent magnetization of each sample was measured and demagnetized using an automatic fluxgate spinner magnetometer to identify a stable magnetization that was then used to restore the original geographic position. Stepwise alternating-field demagnetization up to 45 mT was performed and the magnetic direction was analyzed using a vector endpoint diagram. Samples that failed to yield a stable magnetization were rejected for paleocurrent analyses, but were used for AMS analyses. Consequently, 223 samples were reoriented using magnetic remanence to dipole direction. Normally magnetized samples were oriented to the north (0°), and reversely magnetized samples were oriented to the south (180°) horizontally. After demagnetization, the AMS of samples was measured using a magnetic susceptibility meter (Kappabridge KY-2) at the University of Hawaii (Table 1). In this paper, I use the following parameters to describe the orientation of the magnetic fabric:

$L = K_{max}/K_{int}$ (Balsey and Buddington, 1960),
$F = K_{int}/K_{min}$ (Stacey et al., 1960),
$q = (K_{max} - K_{int})[0.5(K_{max} + K_{int}) - K_{min}]$ (Granar, 1958),

where K_{max} is the maximum axis, K_{int} is the intermediate axis, and K_{min} is the minimum axis of the susceptibility ellipsoid.

RESULTS AND DISCUSSION

Orientation of the Magnetic Fabric

Flinn-diagrams (*L* vs. *F,* Fig. 1) for all measured samples generally show distributions along the abscissa (*F* axis), indicating oblate ellipsoid dominance, although samples close to the point of intersection show shifting toward the ordinate (*L* axis). These later fabrics represent a more spherical and nonpreferential alignment of grains. To observe the shape of the fabric in detail, downhole profiles in each hole are used (Fig. 2). They cover lithostratigraphic Units I and II, from Pleistocene to late Paleocene time.

[1]Whitmarsh, R.B., Sawyer, D.S., Klaus, A., and Masson, D.G. (Eds.), 1996. *Proc. ODP, Sci. Results,* 149: College Station, TX (Ocean Drilling Program).
[2]Ocean Research Institute, University of Tokyo, 1-15, 1-chome, Minamidai, Nakano-ku, Tokyo, 164, Japan. kanamatu@ori.u-tokyo.ac.jp.

Table 1. AMS and paleomagnetic results.

Core, section, interval (cm)	Depth (mbsf)	L	F	P	Pmag D (°)	Pmag I (°)	K_{max} D (°)	K_{max} I (°)	K_{int} D (°)	K_{int} I (°)	K_{min} D (°)	K_{min} I (°)
149-897C-												
2R-1, 55–57	60.45	1.007	1.029	1.036	158.7	52.7	81	0	351	6	174	84
2R-2, 18–20	61.58	1.002	1.013	1.015	79.7	30.5	270	0	0	24	180	66
3R-1, 65–67	70.25	1.008	1.015	1.023	330.2	71.7	241	2	331	13	144	77
5R-1, 67–69	89.57	1.004	1.031	1.035	39.1	27.3	98	2	8	6	204	83
6R-1, 66–68	99.16	1.004	1.036	1.041	328.3	19.4	91	4	182	2	298	86
7R-1, 49–51	108.69	1.003	1.028	1.031	180.5	67.1	89	20	346	30	207	53
8R-1, 120–122	119.10	1.007	1.018	1.025	221.3	-57	269	17	9	30	153	55
11R-2, 22–24	147.31	1.002	1.005	1.007	187.4	–58	84	12	352	10	22	74
11R-3, 127–129	149.59	1.007	1.010	1.017	351.1	–50	284	9	16	9	151	77
11R-4, 12–14	149.94	1.003	1.025	1.028	–	–	95	11	185	2	286	78
14R-2, 10–12	177.40	1.010	1.046	1.056	–	–	175	5	84	6	305	83
14R-4, 23–25	180.53	1.006	1.049	1.056	–	–	284	10	15	7	141	78
15R-1, 71–73	186.11	1.009	1.039	1.048	194.8	–72	88	1	178	1	297	89
15R-3, 82–84	189.22	1.004	1.018	1.023	392.5	–60	273	3	3	13	169	76
16R-4, 15–17	199.75	1.004	1.033	1.037	43.3	82.4	281	4	11	3	139	85
18R-1, 43–45	214.83	1.004	1.035	1.039	277.5	–56	71	14	340	5	230	75
19R-1, 41–43	224.51	1.008	1.027	1.035	73.6	–67	293	21	24	3	122	69
19R-2, 61–63	226.20	1.001	1.017	1.018	326.4	–65	0	11	270	0	180	79
19R-3, 17–19	227.27	1.004	1.012	1.016	115.7	–53	14	11	284	1	188	79
21R-1, 141–143	244.81	1.001	1.037	1.038	77.9	–48	326	19	59	9	173	69
22R-1, 84–86	253.84	1.006	1.029	1.036	314.5	–44	86	11	353	17	208	70
22R-2, 109–111	255.59	1.001	1.050	1.052	236.5	–12	23	0	113	2	286	88
22R-5, 9–11	259.09	1.000	1.020	1.021	357.2	–71	321	5	51	7	197	82
24R-1, 111–113	273.41	1.000	1.030	1.030	163.2	–51	293	7	202	5	78	81
24R-2, 33–35	274.13	1.006	1.028	1.035	127.5	–52	0	5	270	0	180	85
25R-1, 24–26	282.24	1.003	1.022	1.025	217.7	–57	269	3	179	1	67	86
28R-1, 79–81	311.68	1.001	1.010	1.012	234	70.3	21	3	290	18	120	72
28R-2, 93–95	313.33	1.004	1.014	1.019	215.6	–65	201	13	302	40	97	48
28R-4, 102–104	316.43	1.003	1.012	1.015	277.6	2.7	212	3	302	12	108	78
29R-1, 55–57	321.05	1.006	1.015	1.021	148.9	–1.4	224	4	133	9	334	80
29R-2, 101–103	323.01	1.002	1.003	1.005	232.3	–35	341	25	250	2	156	65
29R-3, 62–64	324.13	1.004	1.012	1.016	343.8	15.5	343	4	253	9	98	80
29R-4, 43–45	325.44	1.004	1.010	1.013	320.4	43.8	350	6	81	8	225	80
29R-5, 47–49	326.98	1.003	1.021	1.024	229.6	–54	279	13	10	5	120	76
29R-6, 33–35	328.34	1.008	1.025	1.033	66.5	6.8	105	6	13	17	215	71
31R-3, 89–91	343.79	1.003	1.016	1.019	73.2	–21	272	6	5	29	172	60
33R-1, 122–124	360.32	1.002	1.012	1.014	197.5	56.3	351	15	86	16	220	68
33R-2, 13–15	360.73	1.002	1.010	1.012	270.1	44.9	186	11	95	1	359	79
33R-3, 21–23	362.31	1.001	1.005	1.007	108.7	–37	220	9	311	3	61	80
33R-4, 25–27	363.85	1.006	1.005	1.011	357.5	–4.2	248	14	341	12	111	72
33R-5, 120–122	366.61	1.007	1.008	1.015	270.2	61.5	270	0	0	32	180	58
35R-1, 142–144	379.82	1.003	1.005	1.008	332.7	85	90	27	310	57	190	19
35R-3, 126–128	382.66	1.006	1.015	1.021	142.8	–43	270	0	0	0	180	90
37R-2, 135–137	400.65	1.003	1.017	1.020	6	–21	319	5	49	3	168	85
38R-5, 112–114	414.52	1.002	1.016	1.018	332.5	72.9	146	2	236	3	18	87
43R-4, 25–27	460.35	1.005	1.015	1.020	270.6	–14	271	9	179	9	44	77
44R-1, 120–122	466.51	1.007	1.020	1.027	125.5	–4.3	276	2	7	13	178	77
44R-3, 130–132	469.92	1.003	1.019	1.022	34.7	49.7	265	4	356	9	148	80
44R-4, 12–14	469.92	1.003	1.019	1.022	305.6	–35	287	3	18	9	179	80
45R-3, 134–136	479.34	1.000	1.022	1.022	120.1	1.1	53	8	323	0	233	82
46R–1, 20–22	484.80	1.008	1.007	1.014	282.4	–13	247	148	14	34	39	53
47R-4, 16–18	498.86	1.008	1.012	1.020	129.6	–42	277	2	7	5	162	84
47R-6, 14–16	501.84	1.001	1.019	1.020	104.8	45.8	332	14	62	0	152	76
48R-2, 16–18	505.56	1.002	1.015	1.017	354	43.1	262	12	354	11	124	74
48R-3, 9–11	506.99	1.001	1.021	1.023	223	–33	257	7	348	4	106	82
48R-4, 7–9	508.47	1.003	1.025	1.028	86.6	–48	204	5	114	4	342	84
48R-5, 52–54	510.42	1.002	1.026	1.029	228.7	–47	238	15	329	3	68	75
48R-6, 16–18	511.56	1.001	1.024	1.025	337.5	22.4	116	3	26	4	246	85
49R-1, 22–24	513.82	1.002	1.029	1.031	184.4	63.4	285	8	16	6	145	80
49R-2, 80–82	515.90	1.001	1.032	1.034	199.6	–26	238	19	146	4	45	70
49R-3, 110–112	517.70	1.008	1.056	1.064	176.5	–6.3	259	2	349	8	158	82
49R-4, 87–89	518.97	1.002	1.025	1.027	290.7	–27	289	11	22	16	166	70
50R-2, 58–60	525.28	1.003	1.020	1.023	325.6	–3.5	65	6	335	3	222	83
50R-3, 51–53	526.72	1.001	1.009	1.010	279.3	–19	270	2	0	0	93	88
51R-3, 66–68	536.46	1.003	1.014	1.017	95.6	–30	253	8	163	0	72	82
52R-1, 82–84	543.23	1.003	1.037	1.040	39.5	50.3	222	8	132	1	34	82
52R-2, 44–46	544.57	1.001	1.020	1.021	67.3	–1.7	264	13	172	8	52	75
53R-2, 79–81	554.38	1.003	1.019	1.022	19.9	54.3	260	11	170	3	64	78
54R-1, 56–58	562.36	1.006	1.015	1.021	38.2	11.5	106	12	198	9	325	74
55R-1, 146–148	572.96	1.001	1.053	1.055	189.3	53.2	32	2	302	4	152	86
55R-4, 2–4	576.02	1.003	1.058	1.061	177.3	–14	273	4	182	4	50	85
56R-3, 120–122	585.31	1.003	1.032	1.035	174.9	39.8	104	18	11	9	256	70
56R-7, 39–41	590.04	1.007	1.059	1.066	123.8	22.6	324	5	55	8	200	81
57R-2, 53–55	592.73	1.003	1.066	1.068	186.5	41.3	263	3	172	9	12	81
57R-4, 48–50	596.69	1.004	1.039	1.044	355.5	–64	82	10	172	2	274	79
58R-1, 40–42	600.90	1.005	1.032	1.037	270.2	13.6	278	8	8	2	111	81
58R-2, 15–17	602.15	1.012	1.023	1.035	341.1	–14	266	7	357	13	147	75
58R-3, 16–18	603.66	1.002	1.031	1.033	123.3	3	230	6	321	2	72	83
59R-1, 148–150	611.58	1.013	1.024	1.037	168.6	–5.7	5	5	275	6	134	83
59R-2, 36–38	611.97	1.001	1.037	1.037	275.3	–8.3	281	9	12	11	153	75
149-897D–												
1R-1, 83–85	596.83	1.003	1.039	1.041	234.6	–15	80	4	170	8	323	81
1R-4, 30–32	600.81	1.001	1.041	1.042	266.1	–22	0	0	90	1	265	89
2R-2, 76–78	609.06	1.004	1.046	1.050	291.2	–0.9	270	1	0	0	98	89
2R-3, 14–16	609.94	1.003	1.046	1.049	190.8	–55	346	1	256	4	90	86
2R-4, 39–41	611.50	1.003	1.028	1.031	319.2	–2.8	148	2	58	1	311	88
3R-2, 29–31	618.28	1.001	1.041	1.041	313.8	34	177	4	87	1	345	86
3R-3, 99–101	620.49	1.003	1.057	1.060	199.2	12.3	349	1	79	1	206	89

Table 1 (continued).

Core, section, interval (cm)	Depth (mbsf)	L	F	P	Pmag D (°)	Pmag I (°)	K_{max} D (°)	K_{max} I (°)	K_{int} D (°)	K_{int} I (°)	K_{min} D (°)	K_{min} I (°)
149-898A-												
1H-6, 23–25	7.73	1.005	1.007	1.012	109.2	58.8	358	58	96	5	189	31
2H-4, 108–110	14.78	1.003	1.016	1.019	117.8	50.1	69	18	337	7	226	70
3H-4, 135–137	24.57	1.037	1.011	1.049	107.3	–29	247	1	157	4	352	86
3H-6, 63–65	26.85	1.002	1.009	1.011	113.1	4.3	28	44	266	29	155	32
3H-7, 23–25	27.95	1.004	1.012	1.016	115.3	–12	65	50	323	10	225	39
4H-2, 113–115	30.83	1.002	1.009	1.011	197.7	–68	21	66	253	16	157	18
4H-4, 53–55	33.23	1.009	1.004	1.013	123.8	31	350	68	86	2	177	22
4H-7, 10–12	37.30	1.010	1.019	1.030	250.2	–58	83	42	274	48	178	5
5H-1, 135–137	39.05	1.002	1.020	1.022	302.6	–58	68	12	334	17	192	69
5H-3, 143–145	42.13	1.031	1.008	1.039	321.3	–69	58	80	267	9	177	5
5H-5, 146–148	45.19	1.003	1.008	1.011	290	–58	24	48	274	17	171	37
5H-6, 138–140	46.62	1.003	1.011	1.014	309.3	–56	45	38	300	19	190	46
6H-3, 25–27	50.50	1.002	1.014	1.016	63.7	–39	274	5	21	74	183	15
8H-7, 14–16	75.40	1.007	1.005	1.012	130	–40	72	18	304	62	169	21
10H-7, 10–12	94.30	1.003	1.022	1.025	291.5	–62	236	2	146	10	337	80
11H-1, 130–132	96.00	1.005	1.010	1.015	118.1	–67	45	18	315	0	225	72
11H-2, 53–56	96.75	1.004	1.003	1.007	136.5	–43	359	50	258	9	161	39
11H-3, 15–17	97.87	1.003	1.011	1.014	155.4	-78	27	27	297	0	207	63
12H-3, 85–87	108.70	1.008	1.005	1.013	145.9	–54	67	7	334	21	176	68
12H-4, 28–30	109.00	1.006	1.010	1.016	153.5	–48	238	4	148	1	39	86
12H-6, 96–98	112.70	1.006	1.005	1.010	92.1	–69	177	79	318	9	49	7
13H-1, 145–147	115.15	1.005	1.004	1.009	374	–54	265	8	173	9	35	78
13H-4, 120–122	119.40	1.007	1.007	1.013	32.1	–65	73	57	269	32	175	7
14H-2, 105–107	125.76	1.011	1.008	1.019	259.8	–76	280	7	12	17	169	72
14H-3, 116–118	127.39	1.005	1.035	1.041	210.7	–39	282	15	13	3	115	74
14H-4, 78–80	128.54	1.010	1.029	1.039	6.8	–23	39	1	309	0	201	88
14H-5, 21–23	129.47	1.003	1.046	1.050	229.4	–26	97	2	7	1	255	87
14H-6, 20–22	131.01	1.002	1.019	1.021	234.5	–70	277	13	12	21	157	65
15X-1, 129–131	133.99	1.012	1.015	1.027	303.5	–33	2	0	272	4	93	86
15X-3, 89–91	135.50	1.004	1.013	1.016	313.3	–56	83	0	353	4	179	86
18X-5, 83–86	136.59	1.002	1.000	1.003	46.5	–80	341	7	248	24	86	65
19X-1, 77–79	168.57	1.001	1.007	1.008	216.7	–54	31	0	301	12	124	78
19X-2, 34–36	169.40	1.002	1.007	1.008	232.8	–57	5	0	275	12	97	78
19X-5, 54–56	174.34	1.003	1.015	1.018	204	–52	253	7	344	8	125	79
21X-2, 49–51	188.99	1.006	1.015	1.021	85.9	31.8	258	3	348	6	143	84
22X-1, 90–92	197.60	1.018	1.032	1.050	183.7	–30	189	3	279	0	13	87
23X-2, 103–106	208.93	1.013	1.003	1.016	239.3	–3.8	172	1	265	72	82	18
29X-1, 118–120	265.38	1.002	1.009	1.012	132.4	–2.8	80	3	349	7	193	83
29X-4, 99–101	269.69	1.005	1.025	1.030	0.7	26.9	65	4	185	0	281	86
31X-1, 75–77	284.25	1.002	1.032	1.035	182.7	5.3	79	3	349	2	222	86
36X-2, 95–97	334.35	1.001	1.012	1.012	215.9	8.1	30	55	241	31	142	15
36X-5, 28–30	338.18	1.002	1.015	1.017	66.5	54	90	1	0	0	265	89
149-899A-												
8R-1, 90–92	149.60	1.004	1.016	1.020	189.5	70.5	341	73	11	209	74	
8R-2, 95–98	151.15	1.003	1.039	1.042	232.3	–19	110	0	20	1	204	89
9R-1, 118–120	159.48	1.009	1.049	1.059	307.1	–2.8	334	7	65	11	213	77
9R-2, 80–82	160.60	1.004	1.054	1.058	253.2	47.5	162	5	71	10	280	79
9R-3, 52–54	161.82	1.018	1.021	1.039	207.6	28.6	351	4	260	15	95	74
10R-1, 23–25	168.23	1.004	1.040	1.043	96.2	35.8	283	7	13	4	132	82
16R-2, 97–99	228.37	1.009	1.017	1.026	261.1	27.2	351	4	245	76	81	13
149-899B-												
1R–2, 126–128	233.26	1.013	1.004	1.017	190.7	–17	171	4	58	79	261	10
2R-2, 14–16	236.44	1.002	1.042	1.004	339	–3.7	272	1	2	5	167	84
2R-3, 44–46	238.24	1.004	1.019	1.024	120.1	–7.9	322	18	230	7	120	71
6R-1, 15–17	273.55	1.003	1.011	1.013	244.1	–8.1	295	4	26	11	185	78
10R-3, 56–58	315.56	1.002	1.021	1.024	285.2	49.6	282	5	12	0	104	85
10R-5, 11.9	318.09	1.002	1.019	1.021	269.4	40.2	277	5	186	8	38	81
11R–1, 136–138	322.96	1.002	1.022	1.024	295.7	30.9	254	1	164	5	353	85
13R-2, 84–86	343.24	1.001	1.017	1.018	27.5	–11	320	5	52	14	210	75
13R-4, 70–72	346.10	1.006	1.021	1.027	175.2	28.2	284	4	15	5	160	84
13R-6, 87–89	349.27	1.004	1.052	1.056	295.5	–7.6	277	3	7	5	154	84
14R-1, 141–143	352.01	1.006	1.072	1.079	—	—	42	1	312	8	142	82
15R-1, 114–117	361.34	1.003	1.036	1.039	—	—	78	5	169	8	315	80
15R-2, 91–94	362.61	1.003	1.020	1.023	—	—	272	15	3	4	108	74
15R-3, 57–60	363.77	1.001	1.029	1.030	—	—	254	14	162	8	42	74
149-900A-												
6R-5, 104–106	47.04	1.002	1.067	1.069	248.2	14.7	312	7	43	7	179	80
6R-6, 63–65	48.13	1.005	1.066	1.070	178	47.6	274	3	5	13	170	77
7R-1, 104–106	50.64	1.008	1.009	1.017	276	–27	88	3	179	17	348	73
7R-3, 19– 21	52.79	1.003	1.016	1.019	40.3	–16	255	4	345	4	122	85
8R-1, 14–12	59.42	1.001	1.071	1.072	154.1	–57	256	8	165	1	68	82
8R-3, 86–88	63.16	1.008	1.078	1.087	27.7	–59	77	1	347	4	175	86
9R-1, 137–139	65.87	1.016	1.009	1.026	198.7	45.3	293	18	35	32	179	52
9R-2, 141–143	67.41	1.001	1.009	1.010	346.7	82.4	270	0	0	32	180	58
9R-3, 22–24	67.72	1.004	1.021	1.025	263.4	81.7	265	5	356	12	153	77
10R-1, 100–102	75.10	1.007	1.006	1.012	319.9	70.2	57	83	221	7	311	2
10R-2, 55–57	76.15	1.011	1.005	1.017	145.2	27.3	272	39	68	48	172	12
10R-4, 105–107	79.65	1.003	1.041	1.043	349.3	6.2	325	6	55	2	161	3
11R-3, 61–63	87.31	1.006	1.006	1.012	335.9	–11	259	75	354	2	85	15
11R-4, 126–128	89.46	1.001	1.018	1.019	24.6	–40	314	14	222	4	116	75
12R-1, 26–28	93.66	1.001	1.018	1.019	261	–60	356	9	266	0	173	81
12R-2, 130–132	96.20	1.004	1.021	1.024	191.5	62.4	240	56	35	31	132	12
12R-3, 44–46	96.84	1.005	1.015	1.020	141.1	–39	13	17	280	11	159	70
14R-2, 60–62	114.80	1.001	1.038	1.039	189.8	27.7	296	6	26	6	160	82
14R-3, 108–110	116.80	1.001	1.035	1.036	44.9	–33	278	3	8	6	159	83
14R-4, 107–109	118.30	1.003	1.029	1.032	122.5	–55	46	3	316	5	172	84
14R-5, 7–9	118.80	1.002	1.023	1.024	75.9	–34	189	0	279	4	92	86

Table 1 (continued).

Core, section, interval (cm)	Depth (mbsf)	L	F	P	Pmag D (°)	Pmag I (°)	K_{max} D (°)	K_{max} I (°)	K_{int} D (°)	K_{int} I (°)	K_{min} D (°)	K_{min} I (°)
14R-6, 126–128	121.50	1.001	1.012	1.014	291.6	49.3	293	3	23	1	139	87
14R-7, 25–27	122.00	1.001	1.003	1.004	328.5	28.2	30	65	162	17	257	18
15R-1, 42–44	122.80	1.002	1.010	1.012	196.8	–33	223	21	325	30	103	53
15R-3, 13–15	125.50	1.001	1.007	1.008	239.1	–46	45	5	315	0	224	85
16R-4, 60–62	137.10	1.001	1.001	1.002	274.1	52.8	0	36	270	0	180	54
16R-5, 130–132	139.30	1.005	1.001	1.005	44.6	–68	0	0	90	9	269	81
16R-6, 34–36	139.80	1.000	1.003	1.004	53.7	43.9	88	87	211	2	301	3
17R-1, 117–119	142.84	1.002	1.004	1.006	107.5	–9.5	357	3	88	20	258	70
17R-2, 4–6	143.10	1.003	1.006	1.009	—	—	92	12	360	12	227	73
17R–03, 24–26	144.80	1.002	1.006	1.008	—	—	283	10	14	5	131	79
18R-1, 40–42	151.70	1.007	1.013	1.021	—	—	260	4	170	4	33	84
19R-1, 117–119	162.07	1.009	1.019	1.028	—	—	91	3	182	10	342	80
19R-2, 61– 63	163.00	1.004	1.014	1.019	—	—	271	3	2	10	166	80
20R-3, 142–144	175.02	1.005	1.006	1.011	—	—	271	8	181	4	64	81
20R-4, 22–24	175.32	1.003	1.008	1.011	—	—	93	2	2	3	216	82
20R-7, 63–65	180.23	1.009	1.013	1.022	—	—	267	8	358	11	142	77
21R-1, 132–134	181.62	1.008	1.014	1.022	—	—	277	0	7	16	186	74
21R-3, 40–42	183.70	1.003	1.012	1.015	—	—	264	3	174	2	52	86
21R-4, 113–115	185.93	1.004	1.012	1.016	—	—	86	2	355	9	186	81
22R-4, 107–109	195.47	1.006	1.012	1.018	—	—	272	10	181	7	53	78
22R-6, 39–41	197.79	1.005	1.015	1.020	—	—	97	2	7	2	243	87
24R-1, 69–71	209.89	1.005	1.010	1.015	—	—	115	112	206	2	305	77
24R-2, 39–41	211.09	1.007	1.009	1.016	—	—	277	7	9	11	156	77
24R-4, 27–29	213.97	1.005	1.007	1.012	—	—	100	3	190	12	358	78
24R-6, 34–36	217.04	1.007	1.007	1.014	—	—	265	11	355	2	96	79
25R-1, 135–137	220.15	1.010	1.001	1.011	—	—	274	0	4	14	183	76
25R-3, 63–65	221.16	1.004	1.015	1.019	—	—	97	1	7	4	205	86
25R-4, 125–127	224.55	1.004	1.011	1.016	—	—	271	5	2	5	136	83
25R-5, 127–129	226.07	1.001	1.012	1.013	—	—	291	3	21	9	180	80
26R-2, 20–22	230.10	1.006	1.014	1.020	—	—	274	2	5	5	159	85
26R-3, 24–26	231.64	1.003	1.015	1.018	—	—	92	5	1	12	206	77
26R-5, 15–17	235.15	1.002	1.006	1.009	—	—	259	56	21	19	121	26
27R-1, 103–105	238.51	1.003	1.022	1.019	—	—	112	23	210	19	337	59
27R-5, 33–35	245.06	1.003	1.023	1.026	—	—	69	4	160	12	319	77
27R-6, 49–51	245.93	1.003	1.046	1.049	—	—	91	0	181	7	357	83
28R-5, 101–103	254.99	1.003	1.052	1.055	—	—	260	1	170	1	38	89
29R-1, 59–61	256.31	1.006	1.049	1.055	—	—	90	9	360	1	266	81
29R-5, 65–67	263.97	1.004	1.040	1.044	—	—	76	0	346	1	179	89
30R-5, 100–102	264.74	1.003	1.042	1.046	—	—	83	5	173	4	305	84
31R-1, 95–97	277.13	1.006	1.047	1.053	—	—	88	4	358	3	233	85
31R-5, 39–41	283.45	1.002	1.027	1.030	—	—	78	4	169	8	324	81
32R-6, 118–120	293.34	1.004	1.042	1.045	—	—	277	3	7	5	153	84
33R-4, 141–143	300.99	1.003	1.050	1.053	—	—	115	4	24	4	246	85
34R-1, 117–119	306.61	1.002	1.021	1.023	—	—	276	3	185	2	67	87
34R-4, 112–114	310.76	1.002	1.043	1.045	—	—	153	11	245	7	7	76
35R-1, 77–79	316.42	1.005	1.019	1.025	—	—	256	3	346	2	114	86
36R-2, 143–145	327.70	1.003	1.048	1.051	—	—	101	5	11	2	257	85
36R-4, 122–124	330.52	1.003	1.019	1.022	—	—	111	2	21	2	255	87
37R-2, 70–72	336.82	1.002	1.032	1.034	—	—	267	4	357	2	117	85
37R-4, 38–40	338.20	1.004	1.022	1.026	—	—	97	4	6	12	206	78
38R-2, 61–63	345.33	1.002	1.018	1.020	—	—	101	1	11	3	203	87
38R-5, 52–54	346.43	1.002	1.019	1.022	—	—	120	2	30	1	285	88
39R-1, 46–48	355.20	1.003	1.049	1.051	—	—	97	3	7	1	249	87
40R-1, 98–100	364.82	1.002	1.019	1.021	—	—	93	7	184	8	322	80
40R-2, 55–57	365.98	1.005	1.031	1.036	—	—	126	2	217	1	338	87
41R-4, 124–126	378.32	1.003	1.022	1.025	—	—	262	1	172	1	17	88
42R-5, 138–140	389.01	1.003	1.040	1.042	—	—	63	2	153	5	314	85
43R-1, 35–37	393.98	1.001	1.020	1.021	—	—	139	9	78	6	286	80
44R-5, 9–11	408.87	1.001	1.041	1.042	—	—	64	2	154	9	321	81
49R-1, 127–129	450.81	1.002	1.022	1.024	—	—	82	0	352	3	179	87
50R-5, 61–63	466.36	1.001	1.008	1.009	—	—	220	5	130	4	358	83
51R-3, 103–105	473.51	1.002	1.013	1.015	—	—	267	3	177	7	22	82
52R-6, 11–13	487.00	1.001	1.017	1.018	—	—	134	6	226	13	20	75
53R-3, 128–130	492.87	1.003	1.014	1.017	—	—	106	2	196	2	334	87
56R-1, 93–95	519.30	1.003	1.019	1.022	—	—	73	9	164	8	296	78
60R-3, 86–89	560.22	1.003	1.029	1.035	—	—	225	14	317	9	79	74

Note: L = magnetic lineation, F = magnetic foliation, P = degree of anisotropy, Pmag D = paleomagnetic declination, Pmag I = paleomagnetic inclination, K_{max} D = declination of maximum axis of susceptibility ellipsoid, K_{max} I = inclination of maximum axis of susceptibility ellipsoid, K_{int} D = declination of intermediate axis of susceptibility ellipsoid, K_{int} I = inclination of intermediate axis of susceptibility ellipsoid, K_{min} D = declination of minimum axis of susceptibility ellipsoid, K_{min} I = inclination of minimum axis of susceptibility ellipsoid.

In Holes 897C and 897D, the values of parameter L range from 1.00 to 1.01 and are fairly uniform (Fig. 2). No linear downcore increase is observed in F value. F values at intervals within Unit I and the lower part of Subunit IIC range from 1.00 to 1.07. Conversely, F values of Subunit IIB and the upper portion of Subunit IIC are fairly low. The inclination of K_{min} shows a reversed trend against F value. The inclination of the K_{min} axis ranges from 60° to 90°, but an interval of Subunit IIB (300-360 mbsf) shows shallower and varied inclinations. Undisturbed fine sediment should show foliation and K_{min} inclination perpendicular to the bedding plane. The fabric of low F value and shallow K_{min} inclination suggests that the fabric was disturbed after deposition. A distinct offset is observed at the boundary between Units I and II (300 mbsf). At the same horizon, the porosity trend also shows an offset (Sawyer, Whitmarsh, Klaus, et al., 1994). Although the porosity generally decreases downhole because of compaction, the F value shows no downcore change. This suggests that the magnetic foliation is not developed by compaction. The correspondence of offset horizons may be an important indicator of sediment properties.

Unit I from Site 898 shows fairly low F values, ranging from 1.00 to 1.02. However, F values in Unit II are scattered from 1.00 to 1.06. The K_{min} inclination is negative, coincident with the trend of the F value. The low F values are interpreted to indicate postdepositional

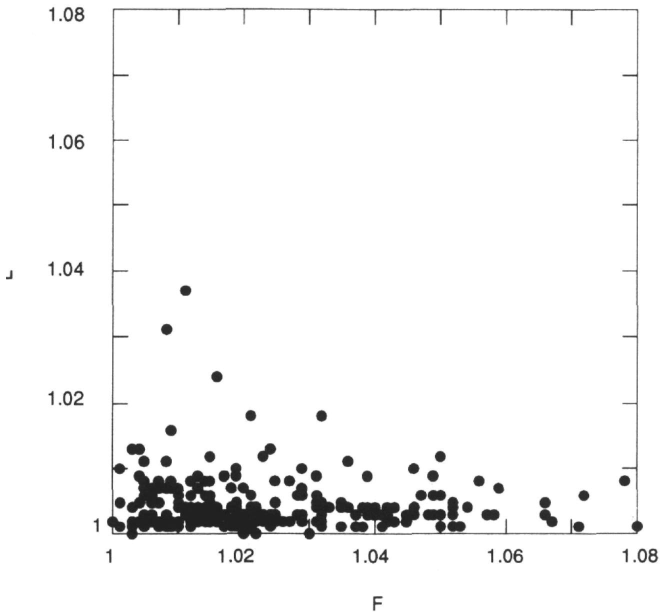

Figure 1. Flinn-type diagram of sediment from Units I and II at Sites 897, 898, 899, and 900. *F* and *L* correspond to K_{int}/K_{min} (foliation) and K_{max}/K_{int} (lineation), respectively.

disturbance as discussed above. Data from Hole 899 are inadequate and do not allow vertical fabric variations to be interpreted.

At Site 900, low *F* values are observed in the intervals between 120 and 230 mbsf and between 440 and 560 mbsf. *F* values are scattered in the intervals between 250 and 400 mbsf and above 100 mbsf. A distinct offset in *F* values at 250 mbsf corresponds to the lithostratigraphic boundary between Subunits IIA and IIB (234.3 mbsf), and at this horizon, the porosity trend shows the reverse offset to that of the *F* value. The interval between 440 and 560 mbsf shows an interesting change in *F* value trend. The trend of *F* value seems to be offset, whereas the slope of the porosity trend changes slightly. The change in sediment property may be related to an unconformity, inferred by the absence of a lower Oligocene microfossil zone (Sawyer, Whitmarsh, Klaus, et al., 1994) at about 470 mbsf.

Two characteristic *F* value intervals are observed at each site: a fairly low *F* interval (1.00-1.02), and a scattered and higher *F* value interval (1-1.07). Except at Site 900, the low *F* value intervals are characterized by shallow K_{min} inclination, which suggests that the fabric was disturbed after deposition. Bioturbation may have destroyed the sedimentary fabric. Subunit IIA of Hole 897C, which shows disturbed fabric, also shows intensive color mottling of *Zoophycos, Chondrites,* and *Planolites*. However, the bioturbation in Units I through II is commonly observed to a varying degree, which is not strong evidence that the low *F* value is the result of bioturbation. Drilling disturbance may have occurred at Site 898. The upper portion of Unit I at Site 898 is clearly disturbed, especially the first 17 cores (0-158.1 mbsf). Most structures are smeared out. The scattering of the porosity data above 50 mbsf probably indicates drilling disturbance.

Tectonic disturbance can also affect the observations. In Units I and II, some cases of structural deformation were observed. Cores 149-900A-26R and 27R (234.1-240.0 mbsf) contain faulted and folded beds that were formed before sediment burial (Sawyer, Whitmarsh, Klaus, et al., 1994). At this interval, only two shallow K_{min} inclination data are observed and these may show tectonic contributions. However, the low *F* values in other intervals are not of tectonic origin.

Intervals of low *F* value and high K_{min} inclination at Sites 897 and 898 are characterized by disturbed fabric. The evidence of disturbance from low F value intervals at Site 900 is not supported by K_{min} inclination observations. The K_{min} fabric inclination is a statistical measurement, so it is possible for fabric subject to weak disturbance to show normal K_{min} inclination, but low foliation.

The variations of *F* value show clear trends and offsets. Some of the changes correspond to lithologic unit boundaries.

AMS Direction

The fabric direction observed throughout Units I and II is of various origins, which include current, gravity, and disturbed orientation. As mentioned in the previous section, the lineation factor is not well developed, but may provide some information about paleocurrent. It is important to select the most suitable measure of fabric for paleocurrent analysis. The fabric signature resulting from gravity during deposition does not produce a preferred K_{max} direction, but this random component will blur the current analysis. The *q* parameter was chosen because it eliminates the gravity origin fabric. The *q* value of gravity induced orientation is typically less than 0.2 (Taira, 1989).

The inclination of K_{min} is used to reject samples affected by postdepositional disturbance. To remove the disturbed fabric, I chose the samples with K_{min} inclination greater than 60°. After selection, only 45 samples were obtained for paleocurrent analysis. AMS directions oriented by remanent magnetization of Unit I from Holes 897C, 898A, and 900A reveal clustering of K_{max}. The magnetic lineation of each hole indicates a general eastward dip, suggesting imbrication of grains (Fig. 3). The AMS directions show a westward trend, but are diverse, probably reflecting the variability of local settings. Unit I in Hole 900A shows a northeast downslope direction, probably caused by turbidity currents from the continental slope (Fig. 4). The submarine canyons around Site 898 are elongated in a west-east direction. The elastics of lower to upper Pleistocene turbidites were probably supplied through this canyon system. Site 898 sediments also show a direction concordant with the direction of the canyons. However, samples from Hole 897C seems to show a different lineation. A possible interpretation is that turbidity currents came from the rise of Vasco da Gama Seamount, situated northwest of Hole 897C.

The current directions for Unit II sediments from Holes 897C, 897D, 899A, and 899B seem to be scattered, and it is difficult to infer paleocurrent directions from them. The lithology of Unit II is characterized by turbidite and contourite facies (Sawyer, Whitmarsh, Klaus, et al., 1994). This scatter may be caused by mixed flow directions, reflecting both contourite and turbidite depositional processes.

SUMMARY

1. Two characteristic intervals in magnetic shape are present: a lower *F* value interval (1.00-1.02) and a higher *F* value interval (1-1.07). *F* value trends show offsets that may be correlated to lithologic unit boundaries.
2. The fabric of low *F* value intervals at Holes 897C, 897D, 898A, and 898B shows shallow K_{min} inclination. This suggests that the foliation structure of magnetic fabric is not parallel to the bedding plane. The origin of low *F* value fabric must be postdepositional sediment disturbance.
3. The AMS of fine-grained sediments from Leg 149 provides some paleocurrent information. The magnetic lineation (*L* values) is not as developed in comparison with foliation (*F* values). Only 45 out of 223 reoriented samples provide reliable magnetic lineations. In several cases the AMS directions suggest that the sediment was derived from the Iberia margin.

ACKNOWLEDGMENTS

I thank Dr. Emilio Herrero-Bervera for permitting me to use the AMS system of the University of Hawaii and for useful suggestions. I acknowledge Professor Asahiko Taira for encouraging discussion on this work.

REFERENCES

Balsey, J.R., and Buddington, A.F., 1960. Magnetic susceptibility anisotropy and fabric of some Adirondack granites and orthogneisses. *Am. J. Sci.,* 2:6-20.

Granar, L., 1958. Magnetic measurement on Swedish varved sediments. *Arkiv. Geofys.,* 3:1- 40.

Hrouda, F., 1982. Magnetic anisotropy of rocks and its application in geology and geophysics. *Geophys. Surv.,* 5:37-82.

Sawyer, D.S., Whitmarsh, R.B., Klaus, A., et al., 1994. *Proc. ODP, Init. Repts.,* 149: College Station, TX (Ocean Drilling Program).

Shor, A.N., Kent, D.V., and Flood, R.D., 1984. Contourite or turbidite? Magnetic fabric of fine-grained Quaternary sediments. *In* Stow, D.A.V., and Piper, D.J.W. (Eds.), *Fine-Grained Sediments.* Geol. Soc. Spec. Publ. London, 15.

Stacey, F.D., Joplin, G., and Lindsay, J., 1960. Magnetic anisotropy and fabric of some foliated rocks from S.E. Australia. *Geophys. Pura Appl.,* 47:30-40.

Taira, A., 1989. Magnetic fabrics and depositional processes. *In* Taira, A., and Masuda, F. (Eds.), *Sedimentary Facies in the Active Plate Margin:* Tokyo (Terra Sci. Publ.), 43-77.

Tarling, D.H., and Hrouda, F., 1993. *The Magnetic Anisotropy of Rocks:* London (Chapman and Hall).

Date of initial receipt: 5 December 1994
Date of acceptance: 31 July 1995
Ms 149SR-213

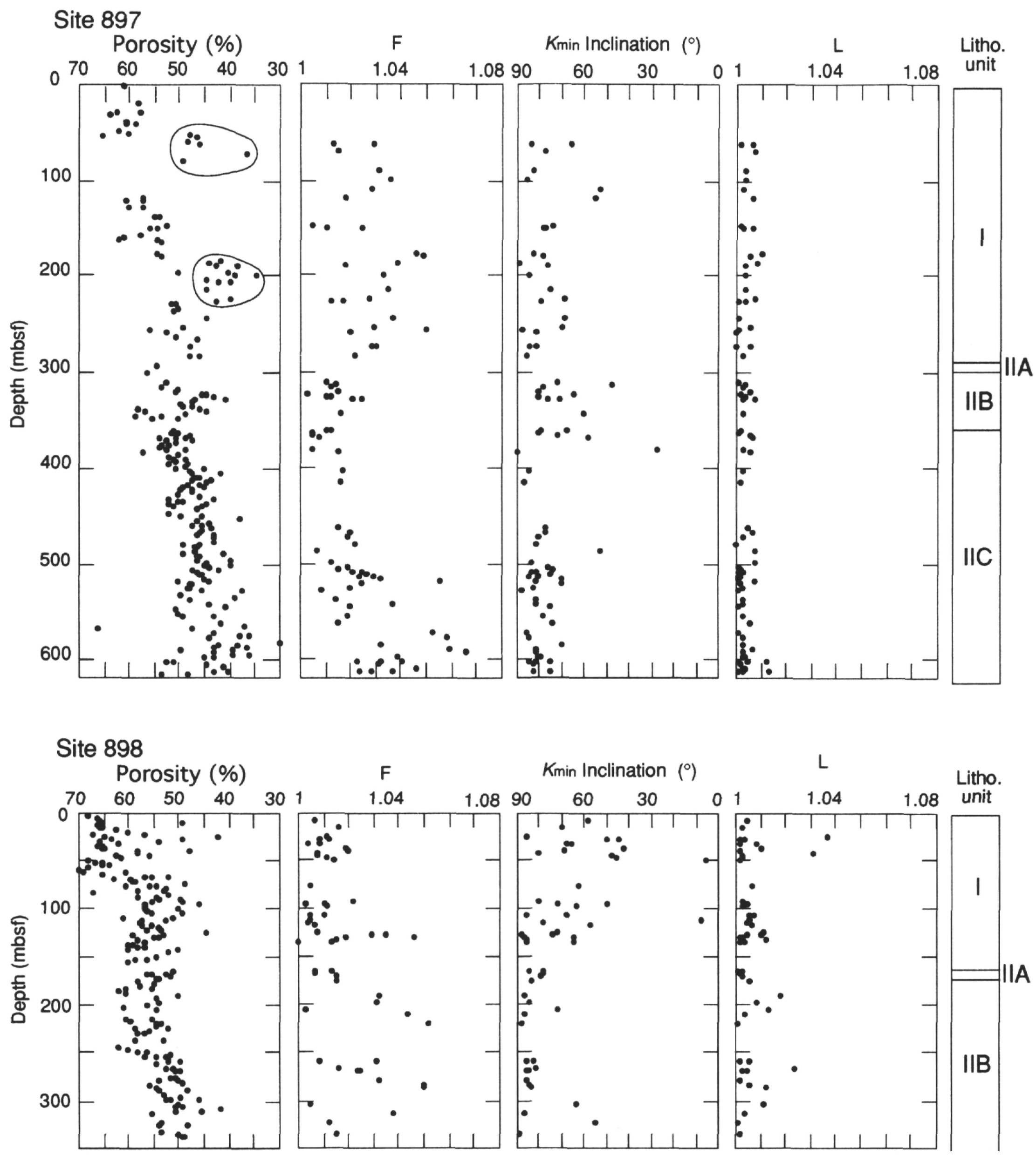

Figure 2. Downhole profiles of porosity, *F* (magnetic foliation), K_{min} inclination, and *L* (magnetic lineation). Porosity data of questionable reliability from Site 897 are circled (Sawyer, Whitmarsh, Klaus, et al., 1994). Litho. unit = lithostratigraphic unit.

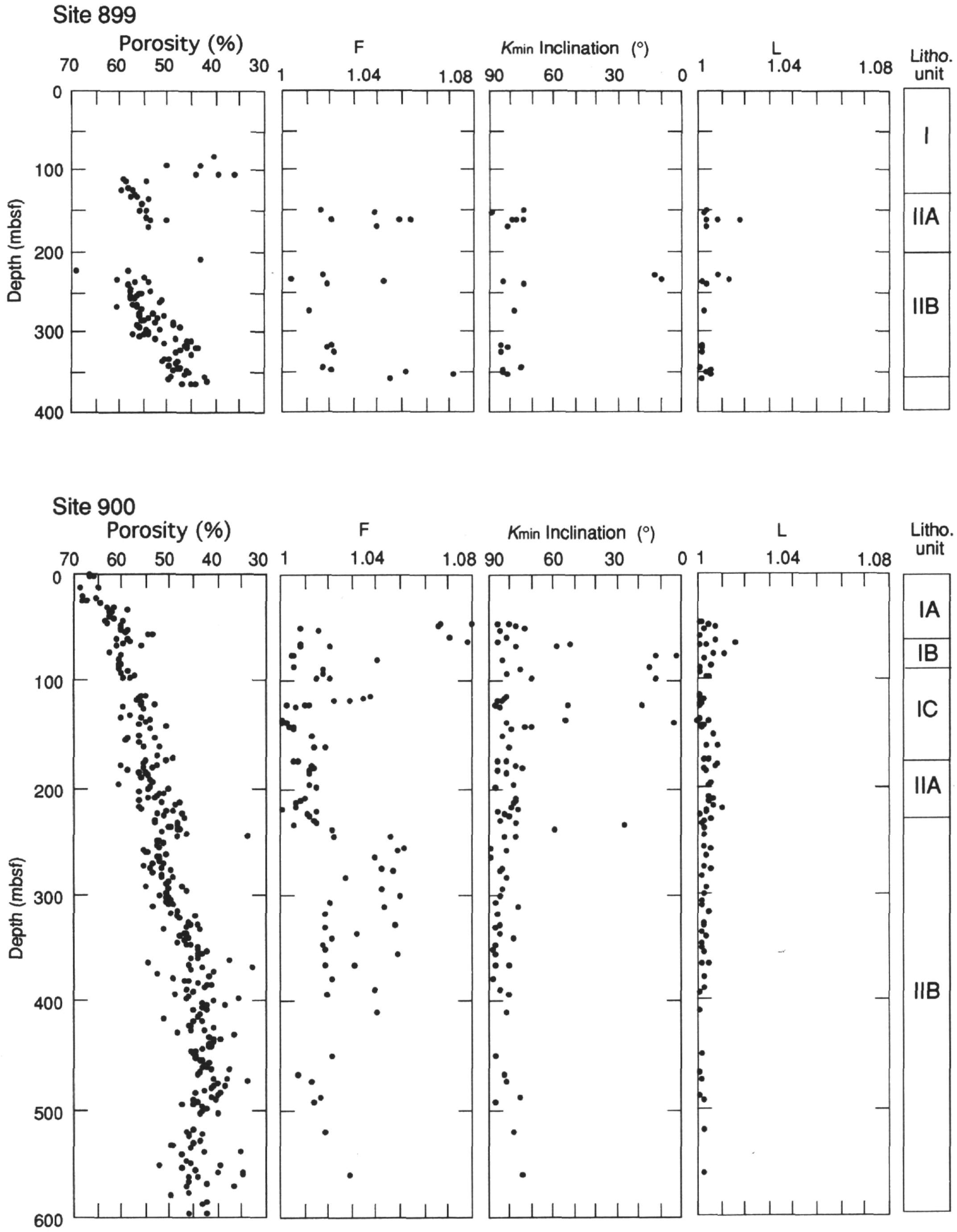

Figure 2 (continued).

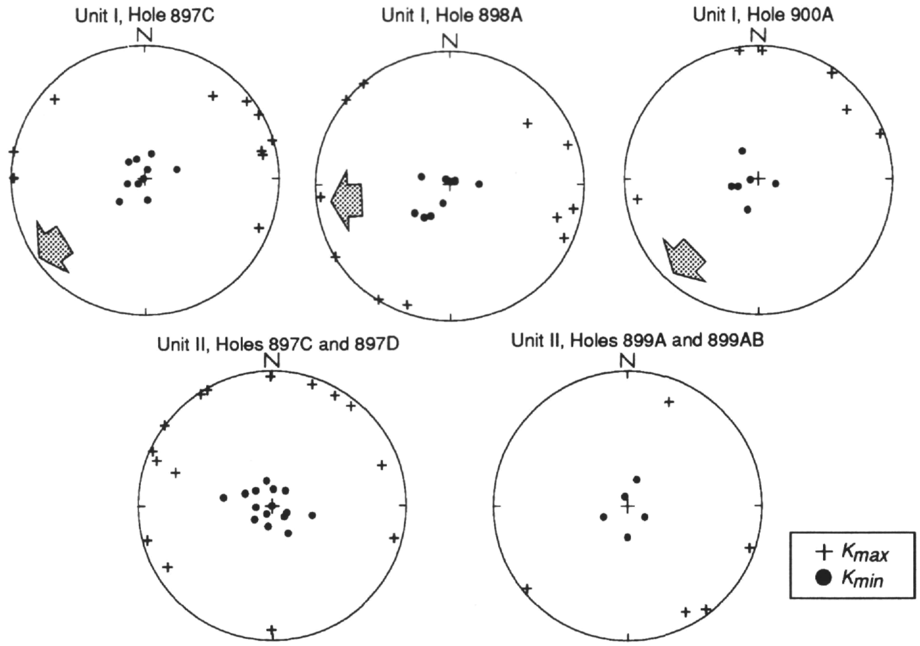

Figure 3. Equal-area lower hemisphere projection of K_{max} and K_{min} axes directions from lithostratigraphic Units I and II. Arrows indicate interpreted paleocurrent directions.

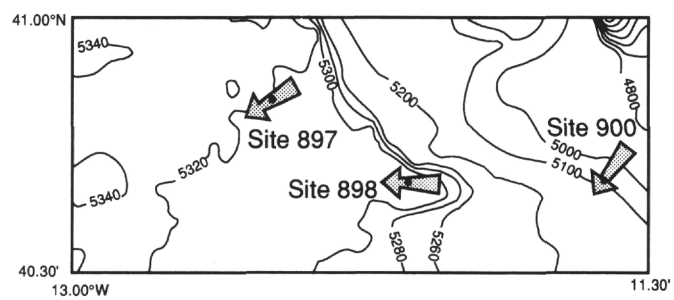

Figure 4. Bathymetry of Iberia Abyssal Plain and possible turbidite currents of Unit I (early to late Pliocene).